ULTRASONIC IMAGING

MICHAEL F. INSANA
University of Illinois
Urbana, Illinois

1. INTRODUCTION

Ultrasonic imaging is a widely used diagnostic technique for examining the dynamic anatomy of mammalian systems safely, inexpensively, and in real time. At its simplest, a low-energy pulse of sound vibrating at frequencies typically between 3 and 30 MHz is introduced into the body by a transducer probe that touches the patient's skin surface. The pulse is attenuated as it travels through tissues, ultimately being converted to heat, and yet a small portion of the pulse energy is scattered back to the probe. The same probe that transmitted the pulse now listens for scattered waves to produce echo signals that are processed to form images. The events outlined above are common components of pulse-echo instruments that can display several types of images, or *sonograms*. Two-dimensional (2-D) anatomical maps are called B-mode (brightness) images. When blood velocity is estimated in 2-D and overlaid onto a B-mode image, a color-flow or C-mode image is displayed. M-mode images display very fast tissue movement, e.g., heart valve motion, along one line of site (vertical axis of the M-mode image) as a function of time (horizontal axis). Similarly, the spectrum of blood cell velocities can be measured along one line of site as a function of time in a spectral Doppler or D-mode display. Generally this information is available to physicians on commercial systems with sub-millimeter spatial resolution and up to 10-ms temporal resolution, although these specifications vary with mode. Zagbzebski (1) provides a clear summary of the basic physics and technology of ultrasonic imaging. More detailed treatments are offered in Refs. 2 and 3.

Physicians examine patients with ultrasound when they suspect a pathology that is known to generate ultrasonic *object contrast*. If regional differences in the tissue properties caused by disease do not alter the image appearance consistently, there is little or no object contrast and reliable diagnosis is impossible regardless of the quality of instrumentation. Physicians are trained to apply the most appropriate technology for the clinical task. They do this by translating their knowledge of disease-induced changes in anatomy and physiology into contrast mechanisms that depend on how energy from the imaging system interacts with the tissues being imaged. Consequently, advances in medicine and biology are great sources of ideas for improving existing imaging methods or developing new approaches to ultrasonic and other types of medical imaging.

Imaging signals are generated from the small portion of mechanical energy emitted by an ultrasonic probe that is backscattered. Scattering sites in tissues are the numerous microscopic surfaces within tissues, e.g., cells, vessels, connective tissue, and other locations where the acoustic impedance abruptly changes.[1] In echocardiography, the echogenic heart muscles appear as bright regions because collagen and elastin near myocytes scatter ultrasound much more than the fluids surrounding the myocardium. However, lesions (focal abnormalities) often appear in B-mode images as subtle changes in regional image texture brightness. To detect a breast tumor (Fig. 1) or a myocardial infarct, the inflammation, edema, and fibrosis that characterize both conditions change the concentration of collagen and interstitial fluids that either increase or decrease echogenicity in the affected region to produce object contrast.

Ultrasonic object contrast differs from that of other image modalities by the nature of the tissue interaction that generates imaging signals. In x-ray mammography, tumors are observed when the average mass density of tissue in the region increases sufficiently. The same tumor is visible ultrasonically only if it contains greater or fewer *micro-surfaces* that scatter sound. Sonograms do not reveal the average impedance properties of tissue. Consequently, sonography is rarely used in boney or gas-filled regions of the body because the large change in impedance at those surfaces reflects virtually all of the energy. Sound must penetrate a region for images to be formed.

The best imaging situations occur when an acoustic pulse travels through relatively homogeneous media and is only weakly attenuated. Attenuation includes absorption and scattering processes; only the latter provide imaging signals. We can coarsely estimate the loss of acoustic pulse amplitude with depth in tissue using the rule of thumb that 0.5 dB/MHz is lost with every centimeter. For example, the pulse-echo amplitude at 10 MHz (breast imaging) is reduced to 0.3% of the initial value at 5-cm depth ignoring beam diffraction. Unlike that of optical imaging methods, ultrasonic attenuation is dominated by absorption, so only a small portion of the attenuated energy is available for imaging. For an average relative scattering amplitude of 0.01, we require [$20 \log (0.003 \times 0.01) > 90$] more than 90 dB of system dynamic range[2] to faithfully represent the entire range of echo amplitudes over just a 5-cm image depth. Furthermore attenuation losses increase with percent body fat, which demands more dynamic range and lower noise for the system to give diagnostic-quality images at this high frequency. Generally, higher pulse frequencies provide greater spatial resolution but less penetration. Imaging through the subcutaneous fat layer in the breast is further complicated by the change in acoustic impedance at the fat–tissue interface. Such interfaces distort (*aberrate*) the sound beam, making it difficult to keep the energy focused. Consequently, spatial and contrast resolution are reduced. If we can

[1]Acoustic impedance z is the product of mass density ρ and longitudinal sound speed c, $z = \rho c$. This definition is strictly true only for incident plane-waves of sound, but it serves nevertheless to provide important intuition about the sources of object contrast when designing medical ultrasound systems.

[2]Dynamic range is the ratio of smallest echo amplitude that saturates the display to the smallest echo amplitude that produces a signal on the display at the threshold of detection. The dynamic range of most systems exceeds 140 dB.

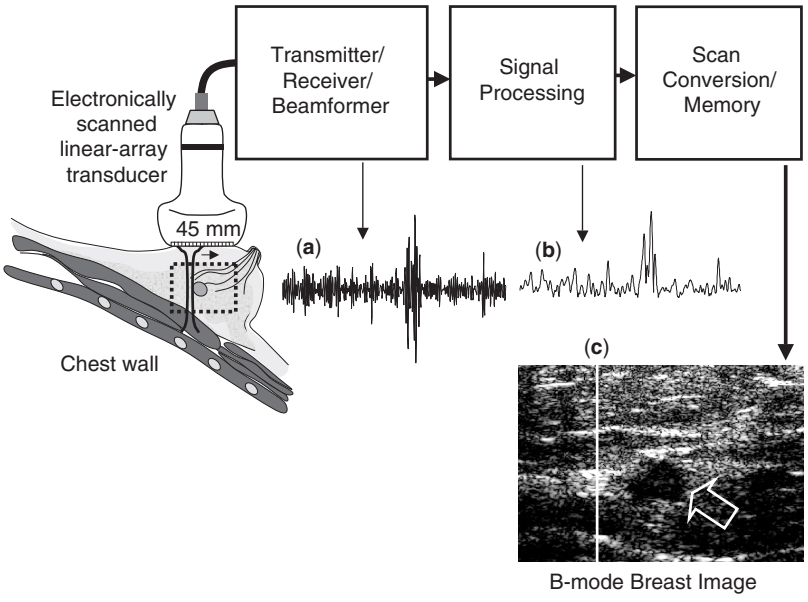

Figure 1. An ultrasonic system for imaging breast tissue is illustrated. A linear array transducer electronically scans and focuses the beam. The progression of one beam through the system from (a) the RF echo signal (b) to the envelope-detected and log-compress signal (c) to a line in a B-mode image is shown. Arrow in the breast sonogram indicates a lesion.

learn to successfully adapt array beamformers to compensate for beam aberrations caused by heterogeneous tissues, diagnostic performance will improve significantly (4). Ultrasonic imaging systems are at their best when imaging persons with low body fat, which provides yet another reason for us to stay slim!

The discussion above introduces just a few of the many challenges faced by researchers and system designers. Further development of ultrasonic imaging requires (1) a more complete understanding of the physics of acoustic energy interactions with tissues; (2) that we apply this knowledge of acoustic physics to image science and thereby better understand what limits object and image contrast, speckle and electronic noise, and spatial and temporal resolution for various patient examinations; and (3) implementation of new instrumentation technologies to improve diagnostic performance in diverse clinical conditions safely and at low cost.

The most successful designs rely on interdisciplinary research collaborations among physicists, engineers, biologists, and physicians who can blend knowledge of pathology, wave physics, tissue biomechanics, modern digital circuitry, and transducer materials to overcome current limitations. The challenge and opportunities both increase with time as knowledge of the molecular basis of disease increases, sensitivity and bandwidth of new transducer materials expands, and the speed and cost of computation improve.

This article does not concentrate on surveying the field of medical ultrasonics; rather, it describes one approach to evaluating the design of a typical B-mode imaging system using a linear array for the purpose of breast imaging. My thinking is that plenty of sources describe the physics and technology but few examples of modeling and evaluating systems for specific clinical examinations, which is where the medical application influences choices about system parameters. System design and evaluation are often the primary goals of biomedical engineering research. The very important topics regarding ultrasonic blood flow imaging systems (3), imaging modes and their designed applications (1), and types of transducer probes (2,5) are left to other treatments.

2. HISTORY

The historical developments of medical ultrasound and associated core technologies have their roots in twentieth century defense and communications engineering. By understanding this development and cleverly applying nineteenth century physics to our twenty-first century knowledge of electronics, materials, and the molecular biology of disease, the role of ultrasonic imaging will continue to grow in medical practice.

Medical ultrasound was born in the 1940s in laboratories throughout Europe, the United States (6) and Japan. The approach and technology was borrowed directly from sonar and radar developments during World War II (7). The first medical applications involved ablation of brain tissue to treat neurological conditions. William Fry at the University of Illinois (8) pioneered what is today the exciting field of ultrasonic surgery for cancer treatment and repair of vascular injuries (9). Simultaneous to Fry's work, investigators at the University of Vienna (10), MIT, and Siemens developed 2-D brain scan imaging techniques. It is interesting to note that there are few current clinical applications of ultrasound in the adult brain, partly because of the difficulty of focusing ultrasound beams through the skull, and the overwhelming successes of computed tomography and magnetic resonance imaging techniques.

The early experiments leveraged several nineteenth century discoveries that included the mathematical theory of wave behavior by Rayleigh and Maxwell, the first electronic amplifiers, and piezoelectric materials discovered by the Curie brothers that allowed the development of ultrasound transducer probes.

Before 1970, scanners used articulated arms that kept track of where the sound beam was pointed to manually scan a 2-D echo field. Images were displayed on bistable (one-bit), black-and-white monitors. During the 1970s, scan converters introduced grayscale imaging (6) that greatly expanded contrast resolution. Mechanical steering of the beam by motor-driven rotation of a focused transducer element speed up echo signal acquisition to the point where real-time (30 frames/s) imaging became possible. Shortly thereafter, one-dimensional (1-D) arrays of transducer elements were introduced (11) that allowed electronically steered and focused beams simply by delaying the times at which individual elements were fired during pulse transmission and echo reception. Linear, curved-linear, and phased-array transducer geometries are now the standard (2). Although it was a major breakthrough to electronically steer and focus arrays, it was soon discovered that care must be taken to avoid imaging artifacts. A seminal paper by Macovski (12) based on Fourier optics (13) provides clear design paths for forming ultrasound beams with an array, and it is standard reading for graduate students studying ultrasonic imaging.

Beamforming is a term that describes techniques for focusing and steering beams emanating from, or received by, an array of sensors. Beamforming fundamentals for ultrasonic imaging are the same as those for sonar and radar imaging; and yet so many details specific to the imaging application remain trade secrets that transducer construction and beamformer designs are still considered an artform. Regardless of future advances in electronics, ultrasonic imaging systems will remain limited by two factors: The speed of sound in the body (average value is 1540 m/s) limits the frame rate, and sound absorption limits the dynamic range and echo signal-to-noise ratio. A corollary limitation is that spatial variations in sound speed and absorption pose formidable challenges to beamforming that, if not overcome, significantly reduce contrast and spatial resolution. The next section describes details of how B-mode images are formed with linear arrays.

3. IMAGE FORMATION

Figure 1 illustrates the basic operations of pulse-echo B-mode image formation with a linear array. The most important components are the piezoelectric elements placed just below the transducer array surface that are the sources and receivers of acoustic energy. Piezoelectricity (literally pressure-electricity) refers to the fact that some ceramics, e.g., lead zirconate titanate (PZT), and polymers, e.g., polyvinylidene fluoride (PVDF), mechanically deform when a voltage potential is placed across opposite parallel surfaces. Like a hammer striking a bell, a shock-excited piezoceramic rings at a resonant frequency determined by its thickness and material properties. Piezo-materials can also be used to sense acoustic fields because they generate a voltage signal with amplitude proportional to the applied acoustic pressure.

The piezoceramic crystal of a 10-MHz, 1-D linear array is about 38 mm long, 10 mm wide, and 0.2 mm thick. The contact area is limited by the need to access small acoustic windows into the body. For example, the transducer in Fig. 2 is composed of 256 elements; each is cut from the same crystal with a 0.02-mm-wide diamond saw. Array elements are coated with an electrically conducting layer and glued to a backing material that provides mechanical support and acoustic damping to increase pulse bandwidth. The elements in this example are $0.15\,\text{mm} \times 0.2\,\text{mm} \times 10\,\text{mm}$.

A short duration, one-cycle (100 ns), 100 VAC amplitude, voltage waveform is applied across the 0.2 mm thickness of a few elements to transmit a pulse as illustrated in Fig. 2 (left). The excited elements vibrate at the resonant frequency for about three cycles (~ 300 ns). Let us excite a 100-element transmit subaperture, which is $100 \times (0.15 + 0.02)\,\text{mm} = 17\,\text{mm}$ long. The transmitted sound beam is circularly focused with a 40-mm radius of curvature by delaying the times that active elements are fired (Fig. 2, left). We have now transmitted a focused 10-MHz pulse with this medium focus, f/2.4 scan-plane aperture geometry.[3]

Touching the array to the skin surface, the acoustic pulse is transmitted into the body. It follows the focused beam path outlined in both figures. Immediately after pulse transmission, the system switches to echo reception (Fig. 2, center). A receive subaperture is similarly selected by activating elements. Received echoes from individual elements are individually amplified (pre-amp), filtered (anti-aliasing), sampled (A/D), delayed (to focus the received energy), amplitude weighted (apodized to suppress side lobes), and summed (Fig. 2, right) to give the beamformed, radio-frequency (RF) echo signal labeled (a) in Fig. 1. Diplexers (Fig. 2, right) protect the receivers from high-voltage transmitters, and time gain compensation (TGC) amplification increases the echo amplitude with depth to partially compensate for attenuation. Post-detection processing includes RF envelope detection (14), labeled (b) in Fig. 1; logarithmic compression; and assignment of gray levels to the resulting envelope amplitude: Regions of low echo amplitude appear as black pixels, and high amplitude regions are bright pixels. Those envelope signals are then positioned in image memory (scan converted) and displayed. Echoes are recorded as a function of time.

These are converted into spatial locations in the scan converter assuming the average sound speed in the body is 1540 m/s. In Fig. 1, the waveform echoes are placed along the white line (c) in the B-mode image. For the linear array geometry in Figs. 1 and 2, the transmit/receive apertures are translated one element spacing (0.17 mm) to the right, and the pulse-echo process is repeated until all image lines of the frame are formed and scan converted for display. In this example, there are 235 lines for a 40-mm-wide image. The entire image frame must be displayed in 33 ms or less to be able to update the information at real-time frame rates.

[3]F-number is defined as the focal length divided by the aperture length. The f-number in this example, $40/17 = 2.4$, is a summary metric of beam focusing used to quantify the lateral resolution of the system.

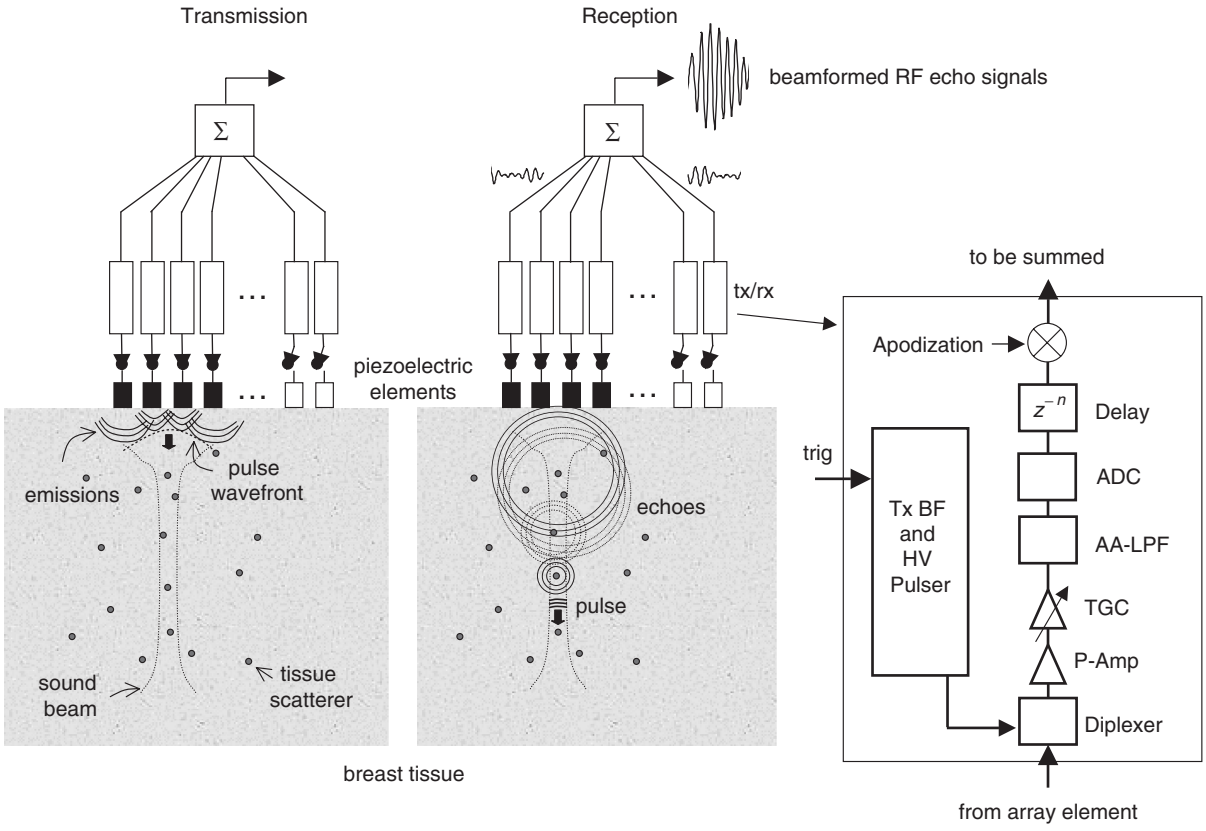

Figure 2. The array–pulser–receiver–beamformer combination from Fig. 1 is diagrammed. Transmission (left) and reception (center) are shown during acquisition of a single echo waveform. Active array elements (black) form the subapertures. An example of one type of transmit/receive (tx/rx) channel is detailed on the right.

4. QUALITY OF THE B-MODE IMAGE

As we proceeded in the example above, I selected parameters typical of current systems. These choices affect image quality, so let us see how well we did. First, it must be said that an objective assessment of image quality requires consideration of the imaging task and application of signal detection theory as detailed in Ref. 15. However, we often rely on engineering figures of merit that summarize five features of the system: resolution, contrast, noise, safety, and cost.

Spatial resolution is a broad term that tells us how close we can position objects of equal echo amplitude and still visualize them as distinct objects. For example, if we can visually distinguish both walls of a 1-mm-diameter artery in cross-sectional view, then we know the system can resolve structures larger than 1 mm at that object contrast. Because spatial resolution in ultrasound depends on the shape and volume of the sound pulse, we now estimate its size in three dimensions.

We begin with the intermediate step of calculating the transmitted pulse dimensions at the focal length. The transmitted *pulse length* is approximated by the product of transmitted pulse duration (0.30 μs in the 10-MHz example above) and the average sound speed in the body; i.e., $0.30\,\mu s \times 1.54\,mm/\mu s = 0.46\,mm$. The pulse length is approximately the same at all depths in the body despite frequency-dependent energy losses, so we say it is *shift invariant*. The smallest transmitted *pulse width* is given by the wavelength of sound in tissue λ times the scan-plane f-number; in our example, $0.15\,mm \times 2.4 = 0.36\,mm$. Similarly, the smallest out-of-plane beam width is found from the transmitted *pulse thickness*: $\lambda \times$ f-number (out-of-plane); i.e., $0.15\,mm \times 40\,mm/10\,mm = 0.61\,mm$. Unlike the pulse length, the pulse width and thickness do vary with depth. The values given above are the smallest pulse dimensions for a focused beam.

The next step is to estimate pulse dimensions after the complete process of transmission, refection, and reception. *The pulse-echo spatial resolution* is what limits B-mode ultrasonic imaging. Let us select transmit and receive apertures of equal size. Then there is a rule of thumb for pulses with Gaussian-shaped amplitudes that enables us to convert the transmit pulse properties to the corresponding pulse-echo properties. Transmitting, reflecting, and receiving such a pulse is described mathematically by a temporal convolution (16). For rectilinear coordinates (x,y,z) where a Gaussian pulse travels along the x-axis, the simplest expression is $\exp(-t^2/2\sigma_t^2) \times \exp(-y^2/2\sigma_y^2) \times \exp(-z^2/2\sigma_z^2)$. The relationship between axial position and measurement time is given by the pulse-echo expression $x = ct/2$. Autocon-

volving this pulse in time only yields $\exp(-t^2/4\sigma_t^2) \times \exp(-y^2/\sigma_y^2) \times \exp(-z^2/\sigma_z^2)$. As the three σ factors define the pulse dimensions, we can see that convolution lengthens the pulse duration by a factor of $2^{1/2}$ and narrows the pulse width in both cross-range dimensions by the factor $2^{-1/2}$. Using the dimensions of the transmitted pulse, we can estimate the best possible (diffraction limited) pulse-echo dimensions at the focal length: $2^{1/2} \times 0.46/2 = 0.33$ mm axially, $2^{-1/2} \times 0.36 = 0.26$ mm laterally, and $2^{-1/2} \times 0.61 = 0.43$ mm elevationally (perpendicular to the image plane). The non-axial pulse dimensions increase in the near-and far-field regions because of wave diffraction (13).

The above values are the best that B-mode spatial resolution can be. It can be degraded, of course, by using a coarse pixel size, low scan-line density, or poor bandwidth displays. As the horizontal scan line increment along the array (0.17 mm) is more than half of the pulse width (0.26 mm), measurable lateral resolution is poorer than the value represented by the pulse width for this system. A smaller horizontal scan line increment is advised in this example, depending on the costs. The best performing systems allow the pulse dimensions to limit spatial resolution. Now you see the vagaries associated with summary figures of merit. Considering that realistic pulses also have side lobes, which we ignored in the discussion above, the concept of pulse width becomes more obscure and estimates of spatial and contrast resolution become coupled. When a rigorous assessment of spatial resolution is required, we recommend that readers use linear-system methods such as modulation transfer function to fully specify imaging properties (15).

Ignoring wavefront distortions from tissue heterogeneities, small f-number-apertures (highly focused beams) are desired to improve cross-range spatial resolution. Yet, as in photography and microscopy, small f-numbers also give a shallow *depth of focus*. The depth of focus is increased with use of multiple transmit foci and *dynamic receive focusing* (1,2). The pulse width can be made to vary slowly with depth, as illustrated in Fig. 2 (left) but often at the cost of a lower frame rate. The principles of dynamic receive focusing are simple. Echoes received soon after transmission are assigned a short focal length and smaller subaperture than those received later in time. Allowing the aperture to grow as the focal length increases with depth keeps the in-plane f-number constant, and thereby it generates a more uniform image texture at the cost of reduced near-field lateral resolution. It is important to have a uniform image texture to avoid mistaking regional changes in system properties for changes in object properties that indicate disease. For example, the hypoechoic region in the breast image of Fig. 1 (arrow) is most likely of clinical significance because we know the system response is fairly uniform throughout the displayed region of interest.

Temporal resolution in sonography is the inverse of the frame rate. In many situations, the video rate of 30 f/s is adequate. However, increasing display depth, number of transmit foci, or line density of the frame beyond certain values requires a reduction in frame rate. The highest rate ultimately is determined by the speed of sound. Considering that each image frame is a temporal sample of the body, it is easy to see that fast body movements, e.g., heart valve motion, will be aliased (1) unless the frame rate is twice the bandwidth of the tissue movement. Modern imaging systems automatically provide the highest frame rate for the parameters selected by the operator; however, it is wise to be vigilant for aliasing artifacts particularly with unusual system configurations common with research applications. The highest temporal sampling is obtained using 1-D M-mode displays.

Noise in sonography is defined as variations in the echo signal that are unrelated to tissue structure. Noise originates from two distinct sources. There is the additive electronic noise from the amplifiers, A/D converters, and other system components. This source is additive because it is independent (or weakly dependent) on the signal amplitude. It is often modeled mathematically as a white Gaussian noise (WGN) process (14), and it is the noise referred to in calculations of echo signal-to-noise ratio (eSNR is defined below).

The textured appearance in the breast image of Fig. 1 is predominantly another type of "noise" called acoustic speckle (17). The two sources are distinguishable because additive noise decorrelates over time, whereas speckle noise does not. Similar to laser speckle, acoustic speckle arises from a coherent summation of reflected waves at the detector surface during reception (Fig. 2, center), and thus it is an inherent property of sonography. Because the bandwidth of the reflected waves is relatively narrow (fractional bandwidth less than 100%) and the detector is sensitive to phase, pressure waves interfere to give the nulls and peaks we see in the B-mode image as speckle. If you look at the very bottom of the breast image in Fig. 1, you will see the smooth surface of the patient's chest wall appear as a broken line, in part, because of speckle. Yet speckle does little to limit our ability to recognize lesions that are large compared with the speckle spot area. In the focal region of the transducer and for random scattering media, the shape of the image speckle equals the shape of the sound pulse in the plane of the image. This is convenient for engineering measurements; however, speckle is a nuisance when trying to assess tissue microstructure. For example, the surface of malignant tumors is often more irregular than that of benign lesions. Speckle can be suppressed with some loss of spatial resolution by *compounding* images (18). In spatial compounding, B-mode images are recorded by viewing the same tissue region from different look angles. Summing images from statistically independent views reduces speckle amplitudes by the square root of the number of images summed. Resolution is lost when the images are not completely spatially registered before being summed and because of asymmetric pulse shapes. Many clinical systems employ compounding techniques under a variety of commercial names.

Contrast is a property of the interaction between tissue and the imaging system. Its definition varies with the task. In sonography, it is usually defined as the ratio of average signal strength in the target region to that in a surrounding region of equal size in decibels (dB). For example, if the average echo amplitude of the lesion in Fig. 1 is half of the amplitude in the surrounding region, it has

an image contrast of $20\log(0.5) = -6$ dB. Object contrast may be greater or lesser than the image contrast depending on image postprocessing parameters. We discussed at the beginning of the article how changes in the body prompted by disease provide object contrast. The image contrast, a property of the imaging system, is often quantified by *contrast resolution* (2). Contrast resolution describes the smallest difference in echo amplitude for two spatially resolvable regions that can be distinguished. Contrast resolution depends on the dynamic range of the instrumentation, bit depth of the A/D converter, eSNR, TGC, and perhaps most importantly, the side- and grating-lobe properties of the array transducers. This rich topic is described in detail by Angelsen (2).

4.1. Safety and Cost

The safety of medical diagnostic ultrasound applied to adults without contrast enhancement is not of concern provided output levels are within the U.S. Food and Drug Administration (FDA) guidelines. After 60 years of clinical applications, there have been no substantiated reports of injury from diagnostic exposures under these conditions. There is a greater potential for cell damage using gas-encapsulated contrast agents because they can lower the intensity threshold for inertial cavitation (19). Simpson et al. have studied many aspects of ultrasonic bioeffects and have recommended statistical methods for assessing risk (20).

Costs depend on the rate of technology development. As the costs of computation and memory decrease and electronic circuits require less size and power, manufacturers can provide more capable systems at constant or lowered costs. One significant aspect of cost is related to the transmit/receive (tx/rx) channel diagrammed in Fig. 2 (right). It is now possible on some systems to provide more than 200 matched tx/rx channels. The result is a faster system with more precise beam control, greater dynamic range, and less additive noise. Such technology has made digital beamformers an industry standard. Also, past systems were built specifically for a particular type of imaging. Today's systems are often PC-based platforms with a great ability to expand and evolve. Consequently, the lifetime and total cost of an investment into an ultrasound system has increased as software and firmware upgrades replace more expensive hardware upgrades.

4.2. System Modeling for Design

The best commercial ultrasound systems automatically reconfigure parameters to deliver the best-possible image quality for each clinical examination. For example, a system optimized for echocardiography looks very different from one optimized for breast cancer imaging because the two examinations demand very different engineering features from the system to achieve their clinical objectives. The exercise outlined above provides readers with a few simple benchmarks for (1) deciding whether a system configuration is appropriate and (2) assessing the effects of proposed modifications for new applications. However, more exacting analyses are often required. There are free public-domain software packages like Field II (21) to help designers simulate beam patterns and whole images. Detailed finite element modeling of piezoelectric materials is possible using various approaches (22), including commercial software packages like PZFlex (23). Bioengineers can assemble these parts using linear system analysis, like that described below, to quickly gain insights into various ultrasonic imaging designs by programming just a few equations in Matlab.

First, we need to specify a mathematical model for tissue scatterers f as a function of position x. Often it is sufficient to assume a random scattering structure given by a zero-mean multivariate-normal process with covariance matrix $K : f(x) = \mathrm{MVN}(0, K)$. Uniform random media are completely specified by the covariance matrix $K = \sigma_f^2 I$, where σ_f^2 is the variance of the scatterer distribution (proportional to the incoherent scattering intensity) and I is a diagonal matrix of ones. If lesion contrast is to be included, then $K = \sigma_f^2(I + S)$, where the diagonal matrix S defines the lesion length/area/volume depending on the dimensionality of the model. Of course, tissue scattering functions are really four-dimensional (4-D) in space and time. However, we are simplifying this discussion by considering reflectors in one spatial dimension that do not move. Extension to 4-D is messy but straightforward.

The object $f(x)$ is a continuous function of position, whereas the beamformed RF echo data are represented by an $M \times 1$ column vector g with elements $g[m]$ that are discretely sampled on the time interval T. If $h(mT,x)$ is the spatio-temporal impulse response of the imaging system (24) and $n[m]$ is an additive WGN sample, then the continuous-to-discrete transformation between object and data space that describes the process of recording echo signals from this idealized medium is (24).

$$g[m] = \int_{-\infty}^{\infty} dx\, h(mT,x) f(x) + n[m]; \quad 0 \le m \le M-1. \qquad (1)$$

When h can be assumed shift invariant, which is reasonable over limited depths where dynamic receive focusing and aperture growth are applied, then h is a function of the difference variable $h(mT - 2x/c)$ (12), and Equation 1 simplifies to a spatial convolution plus noise: $g[m] = (h * f)[m] + n[m]$. To model echo signals in Matlab, it is easier to consider $f(x)$ as an $N \times 1$ vector of spatial samples f and H as an $N \times M$ system matrix whose rows are $h(mT,x)$ for fixed x (15). When h is shift invariant, then H is circulant (15) and straightforward to generate numerically. In matrix form, the ultrasonic imaging equation 1 becomes simply

$$g = Hf + n. \qquad (2)$$

The Matlab code to generate B-mode images via Equation 2 can be found with examples in Ref. 25.

There does not seem to be a standard definition of eSNR in the literature, unfortunately, which means that modelers must be careful in setting their noise levels if they hope to match experimental results. I suggest using

the definition from signal detection theory (14) that defines eSNR as the ratio of the variance for the noise-free signal to that of the noise. In the notation above,

$$\mathrm{eSNR}(x)[\mathrm{dB}] = 10 \log \frac{\sigma_f^2}{\sigma_n^2} \int_0^\infty dt\, h^2(mT, x),$$

where we note that eSNR can vary spatially. eSNR is described further in Ref. 26.

Modifications of Equation 1 or 2 allow us to expand the assumptions and thereby introduce the new aspects of the problem we wish to study. For example, we can add a specular reflecting surface, like the chest wall in Fig. 1, by expanding f to two or three dimensions and giving it a nonzero mean value locally, in a line or plane corresponding to the interface. Note that f remains a column vector regardless of the dimensions of the continuous object f. Examples of modeling specular reflectors in tissues can be found in Ref. 25.

To allow the scattering particles to move in time and space and model flowing blood, we use the object function $f(x', kT_{\mathrm{PRF}})$ in place of $f(x)$ in Equation 1 and then we integrate over x'. This is the situation of a basic Doppler experiment to measure blood velocity (3). T_{PRF} is the measurement time interval between pulse transmissions (inverse of the pulse repetition frequency) for acquiring ensembles of echo waveforms in Doppler analysis (3), and k is an integer. The position of scatterers depends on when and where you "look" at them with the ultrasound pulse. Let the position of a blood cell moving at velocity V at measurement time kT_{PRF} be x'. We can define x' relative to the cell's position at an earlier time $(k-1)T_{\mathrm{PRF}}$, which we call x, from the expression $x' = x + V_x(x, (k-1)T_{\mathrm{PRF}}) \times T_{\mathrm{PRF}}$, where V_x is the component of the velocity vector along the x-axis. Velocity is allowed to vary with position and measurement time to simulate pulsatile flow in vessels. Scattering functions are then computed recursively, $f(x', kT_{\mathrm{PRF}}) = f(x, (k-1)T_{\mathrm{PRF}})$ for $k > 0$, and Equation 1 gives the simulated echo signals.

The equations above have been used to simulate beamformed RF echo signals to explore new blood velocity estimators and coded-pulse excitation techniques for improved estimates of vascular wall shear stress (26) and many other ideas. Provided the imaging system can be described by linear systems analysis (24), Equation 2 is limited only by your ability to translate the physics of an imaging situation into an equation.

5. CURRENT RESEARCH IN ULTRASOUND

Because ultrasound is safe, real time, and relatively inexpensive, sonography in its many forms has become the basis of many new approaches to bioimaging for clinical medicine and basic biological investigations, including molecular imaging. Hundreds of citations each year describe how ultrasound can be adapted to reveal interesting biological processes. Just a few of those applications are summarized below.

Contrast agents are influencing the direction of ultrasonic instrumentation because of their ability to target specific molecular sites for both imaging and drug delivery. There are several approaches, but most contrast media are either gas-encapsulated microbubbles (27) or gas-free nanoparticles (28,29). In both cases, the imaging objective is to enhance the object contrast for specific vascular, cellular, and molecular targets to improve sensitivity and specificity of diagnosis. For example, we see the breast lesion in Fig. 1, but we are hard-pressed to classify it as benign or malignant because both types are hypoechoic. Targeted contrast particles are being manufactured with ligands (molecules that bind to specific cellular receptors) attached to their surface. Bloodborne contrast particles encounter cell receptors and other targeted sites specific to the disease as they circulate (30). Once attached to the target, they may be imaged immediately or they may require chemical or mechanical activation to further enhance contrast and/or to release embedded drugs. In this manner, ultrasound is being used to both image and treat tissues. Intravenously injected microbubbles with fragile shells may not survive multiple passes through the heart and lungs. Stiffening the shells reduces contrast enhancement at diagnostic intensities. Therefore, work is underway to model and measure the dynamic behavior of shelled bubbles in acoustic fields (31) so that the mechanical strength of the shells can be specifically engineered to survive physiological pressures but is programmed to break when necessary in acoustic fields.

One interesting feature of microbubbles is that echoes scattered from these sites are rich in sub- and super-harmonics of the fundamental frequency. That is, a 5-MHz transmit pulse will produce a scattered field at 5 MHz and yet contains significant wave energy at 2.5 MHz and 10 MHz and integer harmonics thereof. This behavior is the hallmark of nonlinear acoustic scattering. Because the bandwidth of transducers has increased substantially in the past decade, it is now possible to filter the echo signals and emphasize harmonic components to isolate microbubble scattering from tissue scattering. The techniques, known collectively as *harmonic imaging*, are most effective at a transmit intensity where the nonlinear scattering response of microbubbles is significant but the nonlinear tissue response is minimal. Other investigators have shown that several transmitted pulse sequences help them improve microbubble contrast while suppressing the tissue response. Such methods were recently reviewed (32).

It should be pointed out that research in the United States on ultrasonic contrast agents lags behind European research because so few agents have received FDA approval and are readily available for purchase without special research agreements.

Other exciting research topics include development of new transducer materials, including single-crystal PZT and piezo-composites that offer enhanced sensitivity, bandwidth, and reduced inter-element crosstalk (5) and Capacitive micromachined ultrasound transducer technology (33). Greater transducer sensitivity allows for higher transmission frequencies to improve spatial resolution, although some newer materials are significantly

more expensive. To improve three-dimensional (3-D) spatial resolution and to record echoes from tissues volumes instead of planes, both at high speed, 2-D linear and phase-array transducers are being tested (34), and some are close to broad commercial release. One formidable technical challenge is to build 2-D array beamformers with enough tx/rx channels that are compact and low power for handheld use. To understand the problem, consider that a fully sampled 100-by-100-element 2-D array requires 10,000 matched channels and at least 20,000 electrically conducting connections! Complexity can be reduced by sparsely sampling the array elements or multiplexing channels. However, these solutions compromise contrast, spatial, and temporal resolutions, so they are now used only in special applications. The industry is waiting for interconnect and VLSI technologies to provide high-density components at low cost. Only then will we see the full potential of 3-D beam steering and focusing for 4-D sonography and color-flow imaging realized.

Finally, elasticity imaging is promising new sources of natural target-specific object contrast not currently available with other imaging techniques particularly for cancer imaging.

6. SUMMARY

The current capabilities of imaging systems and the promises of today's research suggest that ultrasound has a bright future in medical diagnosis and basic biological research. However, continued development faces many challenges that can be solved only through interdisciplinary research. This article described B-mode imaging basics through elementary examples of how designers apply physical and engineering principles to estimate system performance. Although some current research is listed, the intent was to briefly review design principles of interest for bioengineers considering new applications for existing technology or new ultrasonic techniques.

Acknowledgement

The author acknowledges 25 years of stimulating input from students, postdocs, colleagues, and mentors. He is particularly grateful to Kang-Sik Kim, Jie Liu, and Craig Abbey for discussions of topics addressed in this article. The laboratory is currently supported in part by NIH R01 CA082497.

BIBLIOGRAPHY

1. J. A. Zagzebski, *Essentials of Ultrasound Physics*. St Louis: Mosby, 1996.
2. B. A. J. Angelsen, *Ultrasound Imaging.* Trondheim, Norway: Emantec, 2000.
3. J. A. Jensen, *Estimation of Blood Velocities Using Ultrasound: A Signal Processing Approach*. Cambridge: Cambridge University Press, 1996.
4. L. M. Hinkelman, T. D. Mast, L. A. Metlay, and R. C. Waag, The effect of abdominal wall morphology on ultrasonic pulse distortion. Part I. Measurements. *J. Acoust. Soc. Am*. 1998; **104**:3635–3649.
5. K. K. Shung and M. Zippuro, Ultrasonic transducers and arrays. *IEEE Eng. Med. Biol. Mag*. 1996; **15**:20–30.
6. J. Woo (1998). A short history of the development of ultrasound in obstetrics and gynecology (online). University of Oxford. Available: *http://www.ob-ultrasound.net/history1.html*, Accessed July 6, 2005.
7. MIT Staff, *Principles of Radar,* 2nd ed. New York: McGraw-Hill, 1946.
8. J.E. Kennedy, High-intensity focused ultrasound in the treatment of solid tumours. *Nat. Rev. Cancer.* 2005; **5**:321–327.
9. G. ter Haar, High intensity ultrasound. *Semin. Laparosc. Surg*. 2001; **8**:77–89.
10. K. T. Dussik, On the possibility of using ultrasound waves as a diagnostic aid. *Neurol. Psychiat*. 1942; **174**:153–168.
11. C. L. Morgan, W. S. Trought, W. M. Clark, O. T. von Ramm, and F. L. Thurstone, Principles and applications of a dynamically focused phased array real time ultrasound system. *J. Clin. Ultrasound*. 1978; **6**:385–391.
12. A. Macovski, Ultrasonic imaging using arrays. *Proc. IEEE*. 1979; **67**:484–495.
13. J. W. Goodman, *Introduction to Fourier Optics*. San Francisco: McGraw-Hill, 1968.
14. R. N. McDonough and A. D. Whalen, *Detection of Signals in Noise*, 2nd ed. San Diego: Academic Press, 1995.
15. H. H. Barrett and K. J. Myers, *Foundations of Image Science*. Hoboken, N.J.: Wiley, 2004.
16. R. F. Wagner, M. F. Insana, and S. W. Smith, Fundamental correlation lengths of coherent speckle in medical ultrasonic images. *IEEE Trans. Ultrason. Ferro. Freq. Control*. 1988; **UFFC-35**:34–44.
17. R. F. Wagner, S. W. Smith, J. M. Sandrik, and H. Lopez, Statistics of speckle in ultrasound B-scans. *IEEE Trans. Son. Ultrason*. 1983; **SU-30**:156–163.
18. S. W. Smith, G. E. Trahey, S. M. Hubbard, and R. F. Wagner, Properties of acoustical speckle in the presence of phase aberration. Part II: Correlation lengths. *Ultrason. Imaging*. 1988; **10**:29–51.
19. M. W. Miller, D. L. Miller, and A. A. Brayman, A review of in vitro bioeffects of inertial ultrasonic cavitation from a mechanistic perspective. *Ultrasound Med. Biol*. 1996; **22**:1131–1154.
20. D. G. Simpson, M.–H. Ho, Y. Yang, J. Zhou, J. F. Zachary, and W. D. O'Brien, Jr., Excess risk thresholds in ultrasound safety studies: Statistical methods for data on occurrence and size of lesions. *Ultrasound Med. Biol*. 2004; **30**:1289–1295.
21. J. A. Jensen. Field II ultrasound simulation program (online). Technical University of Denmark. Available *http://www.es.oersted.dtu.dk/staff/jaj/field/*, Accessed July 6, 2005.
22. R. Krimholtz, D.A. Leedom, and G.L. Mattaei, New equivalent circuits for elementary piezoelectric transducer. *Electron. Lett*. 1970; **6**:398–399.
23. D. J. Powell, G. L. Wojcik, C. S. Desilets, T. R. Gururaja, K. Guggenberger, S. Sherrit, and B. K. Mukherjee, Incremental "model-build-test" validation exercise for a 1-D biomedical ultrasonic imaging array. IEEE Ultrason. Symp. Proc. 1997: 1669, 1674.
24. R. J. Zemp, C. K. Abbey, and M.F. Insana, Linear system models for ultrasonic imaging: applications to signal statistics. *IEEE Trans. Ultrason. Ferro. Freq. Control*. 2003; **50**:642–654.

25. M. F. Insana, K. J. Myers, and L. W. Grossman, Signal modeling for tissue characterization. In: M. Sonka and J. M. Fitzpatrick, eds, *Handbook of Medical Imaging. Vol 2. Medical Imaging Processing and Analysis*. Bellingham, WA: SPIE Press, 2000.

26. J. K. Tsou and M. F. Insana, Vascular wall shear rate measurement using ultrasound with coded excitation, *IEEE Trans. Ultrason. Ferro. Freq. Control*. In press.

27. P. A. Dijkmans, L. J. Juffermans, R. J. Musters, A. van Wamel, F. J. tenCate, W. van Gilst, C. A. Visser, N. de Jong, and O. Kamp, Microbubbles and ultrasound: from diagnosis to therapy. *Eur. J. Echocardiogr.* 2004; **5**:245–256.

28. S. M. Lanza and S. A. Wickline, Targeted ultrasonic contrast agents for molecular imaging and therapy. *Curr. Probl. Cardiol*. 2003; **28**:625–653.

29. M. J. Zohdy, C. Tse, J. Y. Ye, and M. O'Donnell, Optical and ultrasonic monitoring of laser-generated intracellular contrast agents: Initial cell culture studies. IEEE Ultrason. Symp. Proc. 2004; 1098–1101.

30. J. D. Lathia, L. Leodore, and M. A. Wheatley, Polymeric contrast agent with targeting potential. *Ultrasonics* 2004; **42**:763–768.

31. A. Kvikliene, R. Jurkonis, M. Ressner, L. Hoff, T. Jansson, B. Janerot-Sjoberg, A. Lukosevicius, and O. Ask, Modeling of nonlinear effects and the response of ultrasound contrast micro bubbles: simulation and experiment. *Ultrasonics* 2004; **42**:301–307.

32. P. N. Burns, Instrumentation for contrast echocardiography. *Echocardiography*. 2002; **19**:241–258.

33. O. Oralkan, A. S. Ergun, J. A. Johnson, M. Karaman, U. Demirci, K. Kaviani, T. H. Lee, and B. T. Khuri-Yakub, Capacitive micromachined ultrasonic transducers: next-generation arrays for acoustic imaging? *IEEE Trans. Ultrason. Ferro. Freq. Control*. 2002; **UFFC-49**:1596–1610.

34. O. von Ramm, 2-D arrays. *Ultrasound Med. Biol*. 2000; **26**(Suppl 1):S10–S12.

KEYWORDS

imaging, signal modeling, system design, ultrasound

ABSTRACT

The basic principles of ultrasonic B-mode imaging are summarized. Tissue features that generate contrast and system features that control image quality are reviewed in the context of breast cancer imaging. Approaches to signal modeling, including B-mode and Doppler techniques, are reviewed to guide methodological design and clinical evaluation. The article concludes with a brief summary of current research.

Author Query Form

Title: Encyclopedia of Biomedical Engineering
Article/Number: Ultrasonic Imaging/jwus_Ebs_1233

Dear Author,
During the preparation of your manuscript for typesetting some questions have arisen. These are listed below. Please check your typeset proof carefully and mark any corrections in the margin of the proof or compile them as a separate list. This form should then be returned with your marked proof/list of corrections to John Wiley.

This form should then be returned with your marked proof/list of corrections to N.S. Pandian, Deputy Manager, Macmillan India Ltd., Book Division–IPD, Midford Crescent, New No. 159/1 (Old No. 53/1), Richmond Road, Bangalore-560025, India, Tel: +91-80-51237312; +91-80-51237313, Fax: +91-80-51237310, E-mail: ns.pandian@macmillan-india.co.in

Queries and/or remarks

No Author Query